Forest Ecology and Management 601 (2026) 123370

Contents lists available at ScienceDirect

Forest Ecology and Management

journal homepage: www.elsevier.com/locate/foreco

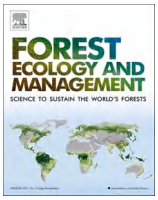

Seaward dynamic changes in mangrove forest over a tide-dominated estuary between 1986 and 2023

Weiming Li [a], Zhijun Dai [a,*], Xuefei Mei [a], Xu Liu [b,*]

[a] State Key Laboratory of Estuarine and Coastal Research, East China Normal University, Shanghai 200241, China
[b] Law School of Guangxi University, Nanning, Guangxi 530004, China

ARTICLE INFO

Keywords:
Mangrove Forest
Seaward expansion
Tide-dominated estuary
Hydro-sedimentary changes
Human Activities
Jiulongjiang Estuary

ABSTRACT

While most of the world's mangrove ecosystems have suffered severe degradation and continued retreat due to human activities and climate change, those located in tide-dominated estuaries have received much less attention. Here, we conducted a comprehensive and systematic exploration of mangroves in the tide-dominated Jiulongjiang Estuary using 1808 Landsat images and regional water and sediment records through the Continuous Change Detection and Classification method. Our results indicate that the mangrove area within the Jiulongjiang Estuary increased substantially by 275 ha, with an average annual expansion rate of 19.55 % from 1986 to 2023. Between 1986 and 1999, the rate of mangrove increase was 3.68 ha/yr, surging to 9.46 ha/yr from 1999 to 2023, despite a brief stagnation from 2006 to 2010. Before 2010, mangrove expansion was mainly concentrated in estuarine bays, while in later years mangroves rapidly colonized the filled estuarine channels. Meanwhile, mangroves have expanded seaward dramatically, with the mangrove shoreline advancing at a rate of 4.36 m/yr. This spatiotemporal pattern of mangrove expansion reflects the combined influence of human interventions and natural estuarine processes. Human activities are the primary driver of mangrove expansion in the study area, with 67 % of the mangroves being planted and predominantly located near the tidal limit. The flood tidal current plays a critical role in fostering a favorable environment for mangrove growth by resuspending sediments and transporting sediments from the outer bay into the channels, both of which promote siltation. Furthermore, the decline in fluvial sediment discharge, wave action, and rising sea levels have not impeded the seaward expansion of mangrove forests. Episodic typhoons have significantly contributed to temporary stagnation in mangrove growth. Human development activities have also caused a portion of mangrove loss. Looking forward, our findings highlight that prioritizing mangrove planting near the tidal limit can better leverage natural sedimentation processes, lower restoration costs, and minimize ecological conflicts, offering valuable insights for mangrove management in tide-dominated estuaries worldwide.

1. Introduction

Amid the catastrophic impacts of global warming, mangroves have gained recognition as critical ecosystems for climate mitigation, capable of sequestering carbon at rates up to 50 times higher than tropical forests (Ferreira et al., 2022; Wang and Gu, 2021; Godoy and Lacerda, 2015; Cummings and Shah, 2017). Primarily found in tropical and subtropical intertidal zones, they provide habitats for diverse species and protect coastlines by enhancing sediment deposition, increasing soil volume, and mitigating waves and storm impacts (Alongi, 2002; Lee et al., 2014; Kamil et al., 2021). During tropical cyclones, mangroves reduce storm surges and wind forces and typically recover afterward, demonstrating their resilience (Krauss and Osland, 2020). Despite their critical ecological functions, mangrove ecosystems have historically been neglected. In the latter half of the 20th century, urbanization, aquaculture, and overexploitation led to the loss of one-third of global mangroves (Alongi, 2002). Between 2000 and 2016, approximately 62 % of global mangrove cover has disappeared (Goldberg et al., 2020). Mangrove ecosystems face significant survival challenges (Feller et al., 2010). Furtherly, mangroves can tolerate a maximum sea-level rate of 7 mm/yr (Lovelock, 2020). If the rate of sea-level rise exceeds this threshold, mangroves may fail to accrete vertically at a sufficient pace, resulting in increased submergence and habitat loss over the next 30 years. (Saintilan et al., 2020).

* Corresponding authors.
E-mail addresses: zjdai@sklec.ecnu.edu.cn (Z. Dai), liuxu@gxu.edu.cn (X. Liu).

https://doi.org/10.1016/j.foreco.2025.123370
Received 29 August 2025; Received in revised form 11 November 2025; Accepted 17 November 2025

Natural drivers strongly influence the habitat conditions, distribution, and health of mangrove ecosystems. Since the 1960s, approximately 36,000 ha of mangroves have been lost due to natural causes (Sippo et al., 2018). Factors such as intertidal elevation (Lovelock et al., 2011) and hydrodynamics (Alongi, 2009) are critical for mangrove survival and establishment. Several natural drivers of mangrove degradation have been clearly identified in existing research, including storms (Temmerman et al., 2023), waves (Sánchez-Núñez et al., 2019), and tides (Lewis et al., 2016; Long et al., 2021). Low-frequency, high--intensity weather events, such as tropical cyclones and extreme climate events, also pose significant threats to mangrove ecosystems (Sippo et al., 2018). Additionally, tidal inundation and waves, through their effects on sediment dynamics, influence the formation of tidal flats and limit the seaward expansion of mangroves (Balke et al., 2015). Especially when wave action is dominant, wave attacks cause damage to the root systems and soil structure of mangroves, leading to the retreat of the mangrove front in the estuary (Allison and Lee, 2004). Riverine sediment provides material for estuarine mangroves, but in river-dominated estuaries, dam construction has caused erosion and mangrove retreat (Malini and Rao, 2004). Tidal currents can partially compensate for upstream sediment deficits, supporting mangrove expansion (Zhou et al., 2024). Up to date, most studies have focused on river-dominated estuaries (Dai et al., 2024; Rahman et al., 2013; Walsh and Nittrouer, 2004), while the understanding of mangrove dynamics in tide-dominated estuaries remains relatively limited by comparison.

Tide-dominated estuaries exhibit distinctive mangrove dynamics. Compared to wave- and river-dominated deltas, the Nanliujiang Delta shows the most pronounced seaward mangrove expansion (Dai et al., 2024). Similarly, despite an overall decline in mangrove area from 81, 979 ha to 54,248 ha in the Fly River Delta, localized seaward expansion has been observed, likely driven by tidal sediment dynamics (Wu et al., 2025). However, in tide-dominated estuaries, these studies generally attribute seaward mangrove expansion to tidal sediment dynamics without providing systematic analyses, leaving long-term patterns and the interactions with external environmental factors largely unexplored. Understanding these processes is ecologically significant, as positive feedbacks between tidal dynamics and mangroves contribute to sustainable coastal systems. Recognizing the hydrodynamic characteristics of tide-dominated estuaries also offers management benefits by reducing reliance on engineered structures and mitigating reclamation-induced ecological conflicts.

Further, anthropogenic activities could be a major contributor to the significant decline in mangrove areas. Human interferences such as coastal development and aquaculture have led to the extinction risk of 16 % of the 70 known mangrove species worldwide (Polidoro et al., 2010). While the focus of mangrove research has been directed toward areas experiencing degradation, studies on regions with expanding mangroves over tide-dominated estuaries have inevitably been limited.

Mangrove ecosystems are predominantly found in muddy intertidal zones (Wu et al., 2022), making them challenging and unsuitable for labor-intensive large-scale observations (Tian et al., 2023). Remote sensing offers a crucial means of obtaining both spatial and temporal data on the distribution of mangrove ecosystems and their ongoing changes (Kuenzer et al., 2011). Tidal fluctuations alter mangrove visibility across tidal stages, posing challenges for remote sensing monitoring. The methods such as Continuous Change Detection and Classification (CCDC) and Continuous monitoring of Land Disturbance, by utilizing long-term time series imagery analysis (Awty-Carroll et al., 2021; Pham et al., 2019), have the potential to reduce the interference of factors like tidal fluctuations. Additionally, open-access mangrove datasets contribute to ecosystem service assessments and support conservation and restoration efforts (Worthington et al., 2020). Many datasets such as upstream suspended sediment concentrations (Long et al., 2021), tidal currents (Zhou et al., 2024), waves, and sea-level rise (Wu et al., 2025) have been widely used to quantify the influence of hydrodynamic factors on mangrove ecosystems.

The Jiulongjiang Estuary, a tide-dominated estuary and mangrove reserve within a densely populated coastal region, faces the dual challenge of balancing intensive human development and mangrove conservation. Despite increasing restoration efforts, the mechanisms sustaining mangrove expansion under strong tidal influence remain poorly understood. This study addresses this gap by quantifying long-term spatiotemporal dynamics of mangrove forests (1986–2023) and disentangling the relative roles of human interventions and hydrodynamic processes, providing new insights into mangrove resilience and sustainable management in tide-dominated estuaries. The primary objectives of this research are: 1) to quantify the temporal and spatial changes in mangrove area within the Jiulongjiang Estuary; 2) to identify the dynamic changes in the mangrove shorelines; and 3) to explore the potential drivers of mangrove expansion and reduction. This research will provide valuable insights into the holistic changes of mangroves in the Jiulongjiang Estuary, offering important guidance for mangrove management in tide-dominated estuaries, restoration efforts, and policy-making worldwide.

2. Materials and methods

2.1. Study area

The Jiulongjiang is the second-largest river in Fujian Province, China. It traverses Zhangzhou before discharging into the Taiwan Strait, opposite Xiamen Bay (Zeng et al.,2022). Located in southeastern China, the Jiulongjiang is a subtropical river strongly influenced by the subtropical monsoon climate. The region experiences pronounced seasonal variability in both precipitation and temperature, with an average annual rainfall of 1400–1800 mm and an average annual runoff of 14.4 billion m^3 (Mo et al.,2016). The flood season extends from May to September, during which approximately 75 % of the annual precipitation occurs. Although this period accounts for only about 24 % of the year, it contributes more than half of the total annual runoff, with seven flood events recorded in 2014, all within the wet season (Gao et al., 2018). In addition to floods, Fujian is one of the provinces with the highest number of typhoon disasters and losses (Wang et al., 2021; Ye et al., 2020), and the Jiulongjiang Estuary is therefore highly exposed to frequent and intense typhoon disturbances.

The study area is situated at the Jiulongjiang Estuary, a macrotidal region where river runoff interacts with tidal currents. The estuary features a typical semidiurnal tidal regime, with an average tidal range of 3.9 m and a maximum tidal range of 6.24 m (Jiang and Wai, 2005; Wang et al., 2013), and is classified as a tide-dominated estuary (Wang and Jiang, 2013). There are narrow tidal sand ridges distributed in the estuary (Xu et al., 2014). The study area, located between 117°47′06″E–117°59′35″E and 24°19′40″N–24°29′45″N, lies at the northernmost limit of mangrove distribution in China (Wang and Gu, 2021).

The Jiulongjiang Estuary is a key mangrove distribution area in Fujian Province, dominated by cold-tolerant species such as *Kandelia obovata*, *Aegiceras corniculatum*, and *Avicennia marina*. These species are well-adapted to the region's climatic conditions. The estuary is recognized as one of the world's primary habitats for *Kandelia obovata* (Wang et al., 2000; Zhang and Lin, 1984). Moreover, in 1988, the Jiulongjiang Estuary mangrove provincial nature reserve was established at the Jiulongjiang Estuary (Fig. 1C). For analysis, the study area is divided into three sections based on the distribution of islands: Northern Section (NS), Central Island Section (CIS), and Southern Section (SS) (Fig. 1).

2.2. Materials

In this study, all available Landsat time-series remote sensing images (Path 119, Row 43; Path 120, Row 43) spanning from 1986 to July 2024 were obtained from Google Earth Engine (GEE) for mapping the spatial distribution of mangrove forests. These images include Landsat 5 TM,

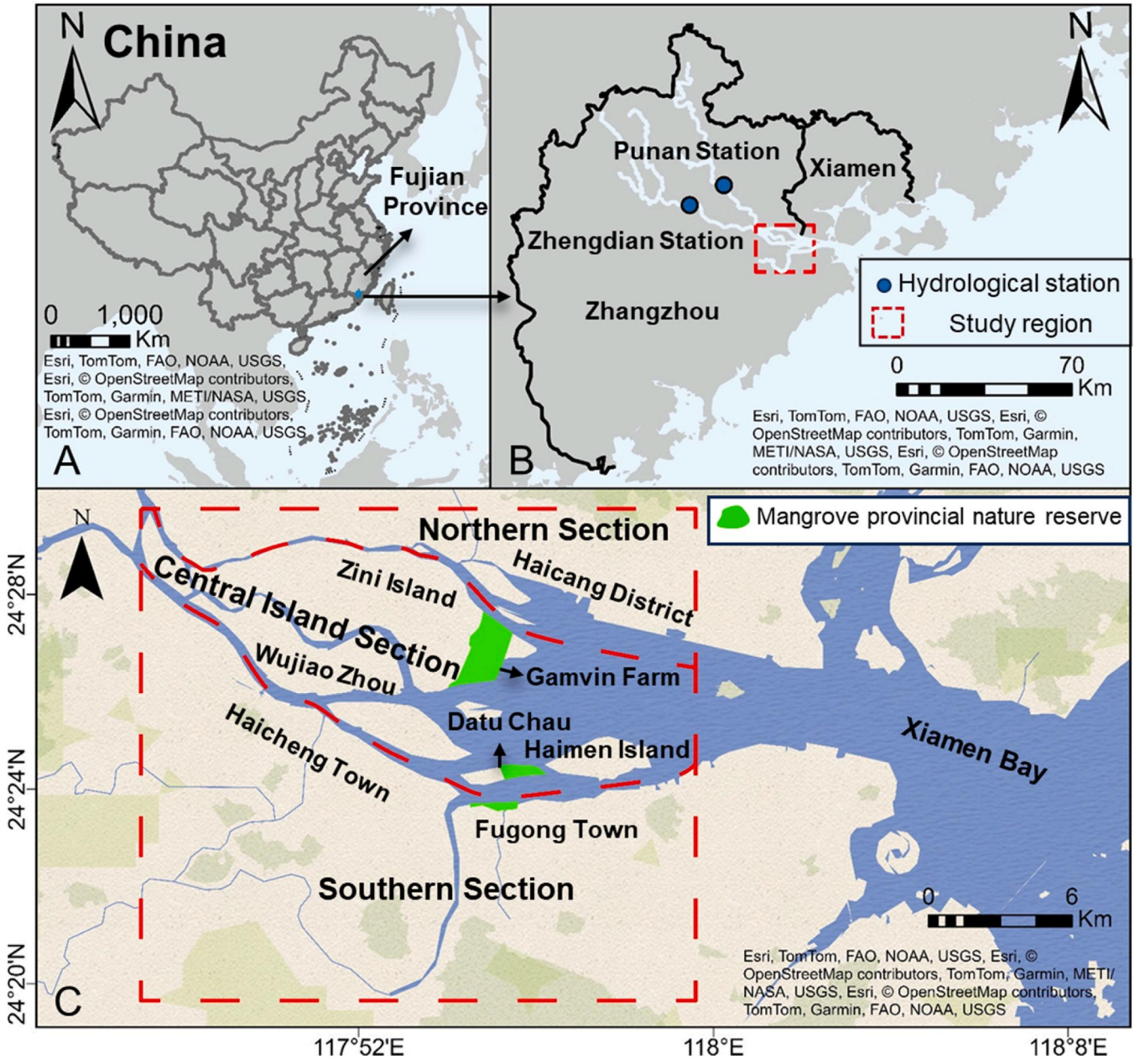

Fig. 1. Spatial setting of the study area in the Jiulongjiang Estuary. (A) Map of China indicating the location of Fujian Province. (B) Distribution of hydrological stations and major mangrove areas within the study region. (C) Division of the study area into three sections: Northern Section (NS), Central Island Section (CIS), and Southern Section (SS).

Landsat 7 ETM+ , Landsat 8 OLI, and Landsat 9 OLI-2, all from USGS Landsat Collection 2, which provides improved geometric accuracy, updated radiometric calibration, and globally consistent terrain correction. The images are referenced to the WGS84 geographic coordinate system and the UTM projection coordinate system. During image preprocessing, the Quality Assessment band was used to eliminate pixels affected by clouds, cloud shadows, and those with abnormally high values due to sensor saturation. The Surface Reflectance Atmospheric Opacity band was employed to remove pixels exhibiting high opacity resulting from atmospheric interference. For Landsat 7 ETM+ data, minor corrections were applied to address scan-line gaps caused by the scan-line corrector failure, thereby eliminating artifacts associated with missing scan lines. A total of 1808 images were processed to generate the mangrove distribution maps.

The Mangrove China_LASAC_sharing (MC_LASAC) dataset was utilized to validate the accuracy of the results (Zhang et al., 2021). Runoff and sediment data were obtained from the Fujian Provincial Water Resources Bulletin, the Soil and Water Conservation Bulletin, and hydrological records from the Punan and Zhengdian hydrometric stations covering the period from 1980 to 2009. For the latter, only average values from 1980 to 1988 were available for the Punan and Zhengdian hydrometric stations, with no data for 1989–1990. Typhoon data were sourced from the National Oceanic and Atmospheric Administration (NOAA) National Centers for Environmental Information (NCEI) (https://www.ncei.noaa.gov/data/international-best-track-archive-for-climate-stewardship-ibtracs/v04r00/access/shapefile/). Sea level data were sourced from the China Sea Level Network. Wave data used in this study were obtained from the fifth-generation atmospheric reanalysis dataset (ERA5) produced by the European Centre for Medium-Range Weather Forecasts (ECMWF) (Hersbach et al., 2018). This dataset provides hourly global wave and climate variables, and the present analysis utilized mean hourly data for 2021–2023 (https://doi.org/10.24381/

cds.adbb2d47).

2.3. Methods

2.3.1. Data preprocessing

The images of data used in this study underwent preprocessing, including atmospheric correction, radiometric calibration, and geometric correction (Dwyer et al., 2018). Spectral indices provide valuable phenological information, which can enhance the accuracy of classification (Siachalou et al., 2017). The reflectance values of blue, green, red, near-infrared, shortwave infrared, and brightness temperature bands were selected, and six spectral indices (Table 1) were calculated for each image to serve as input parameters for the classifier.

2.3.2. CCDC methodology

The Continuous Change Detection and Classification (CCDC) time series modeling and change detection method was proposed by Zhu and Woodcock (2014). CCDC constructs a time series model for each pixel using all available Landsat surface reflectance measurements (Eq. (1)), allowing for the detection of deviations from past patterns in spectral time series data. The classification method, introduced by Zhu et al. (2016) and Pengra et al. (2016), is applied after the change detection step. It uses model coefficients and the root mean square error estimated by the model, among other factors, as inputs for the Random Forest Classifier to perform classification. To improve the robustness, repeatability, and spatial consistency of the algorithm, it is necessary to adjust the CCDC input parameters to better characterize gradual land surface changes (Brown et al., 2020). All parameters from the time series model and change detection outputs, including coefficients and root mean square error, together with other nonlinear variables such as slope and aspect, are used as input data for the Random Forest Classifier in land cover classification. A time-series model was constructed for the imagery from 1986 to July 2024 to perform classification (Fig. S1). Considering that mangroves are evergreen plants (Suratman, 2008), December was selected as the classification period to improve the distinction of mangrove distribution, as most surrounding non-mangrove vegetation exhibits reduced greenness or senescence during winter, thereby enhancing spectral contrast. Using the MC_LASAC dataset, Google Earth historical imagery, and online panoramic maps, five types of sample points—water bodies, intertidal zones, impervious surfaces, mangroves, and other land cover types—were visually interpreted. The training dataset consisted of 80 % of the samples, with the remaining 20 % used for model accuracy testing.

Table 1
Spectral indices used for classification.

	Name	Equation	References
1	Normalized Difference Vegetation Index (NDVI)	$NDVI = \frac{\rho_{nir} - \rho_{red}}{\rho_{nir} + \rho_{red}}$	Zhang et al., (2017)
2	Normalized Difference Mangrove Index (NDMI)	$NDMI = \frac{\rho_{SWIR2} - \rho_{green}}{\rho_{SWIR2} + \rho_{green}}$	Zhang et al., (2017)
3	Modified Normalized Difference Water Index(mNDWI)	$mNDWI = \frac{\rho_{green} - \rho_{SWIR}}{\rho_{green} + \rho_{SWIR}}$	Chen et al., (2017)
4	Mangrove Vegetation Index (MVI)	$MVI = \frac{\rho_{NIR} - \rho_{green}}{\rho_{SWIR1} - \rho_{green}}$	Baloloy et al. (2020)
5	Land Surface Water Index (LSWI)	$LSWI = \frac{\rho_{NIR} - \rho_{SWIR}}{\rho_{NIR} + \rho_{SWIR}}$	Chandrasekar et al. (2010)
6	Enhanced Vegetation Index (EVI)	$EVI = 2.5\frac{\rho_{NIR} - \rho_{red}}{\rho_{NIR} + 6\rho_{red} - 7.5\rho_{blue} + 1}$	Nepita-Villanueva et al. (2019)

$$\hat{p}(i,t) = c_{0i} + c_{1i}t + \sum_{n=1}^{3}\left(a_{ni}\cos\frac{2\pi nt}{T} + b_{ni}\sin\frac{2\pi nt}{T}\right) \quad (1)$$

Where i is the ith Landsat band, t is the ordinal of the date, with January 1 of the year 1 having an ordinal value of 1 (using the proleptic Gregorian calendar), T is the average number of days per year, which is 365.2425, a_{ni}, b_{ni} are the estimated nth order seasonal harmonic coefficients for the ith Landsat band, c_{0i}, c_{1i} are the estimated intercept and slope coefficients for the ith Landsat band, $\hat{p}(i,t)$is the predicted value for the ith Landsat band at the ordinal date t.

2.3.3. Spatial information of mangrove

To assess mangrove gains and losses, the Raster Calculator tool in ArcGIS was used to perform layer addition and subtraction, generating new layers that reflect the spatial distribution of mangrove areas. The output values from these operations indicate areas of mangrove gain or loss.

The Digital Shoreline Analysis System is an effective tool for monitoring shoreline changes in coastal wetlands with high spatial and temporal resolution (López and Cellone, 2022). In this study, mangrove shorelines from 1986, 1990, 1994, 1998, 2002, 2006, 2010, 2014, 2018, and 2023 were visually interpreted and extracted using ArcGIS. To quantify shoreline change, a total of 767 transects were generated perpendicular to the mangrove front at 30-meter intervals along the entire study coastline, spanning five distinct coastal segments, thereby providing sufficient spatial coverage for temporal analysis. The Weighted Linear Regression method was then applied to these transects to calculate the rate and direction of mangrove movement over time.

2.3.4. Landscape pattern

Landscape pattern indices quantify the complex spatial patterns within a landscape, enabling a better understanding of the associated ecological processes through computation (McGarigal, 2006). FRAGSTATS is a versatile, automated program for quantifying landscape structure, offering a comprehensive selection of landscape metrics with minimal technical training requirements (McGarigal and Marks, 1995). Patch Density (PD) reflects the degree of fragmentation in a landscape. A higher density indicates smaller and more dispersed patches. The Path Cohesion Index (COHESION) measures the degree of connectivity between patches in a landscape and is commonly used to assess habitat connectivity. A higher COHESION value indicates better connectivity between patches. These two indices were selected to measure the mangrove landscape pattern. The formulas for these indices are as follows (McGarigal and Marks, 1995):

$$PD = \frac{N}{A} \quad (2)$$

$$COHESION = \left[1 - \frac{\sum_{i=1}^{n} p_i}{\sum_{i=1}^{n} p_i\sqrt{a_i}}\right]\cdot\left[1 - \frac{1}{\sqrt{N}}\right]^{-1}(100) \quad (3)$$

Where, N: total number of patches of the selected patch type landscape, A: total area of the landscape, i: 1, …, n patches, ai: the area of patch i, p_i: the perimeter of patch i.

2.3.5. Datasets and statistical analyses

To better interpret the observed mangrove dynamics, we incorporated multiple datasets related to sediment supply, tidal characteristics, wave conditions, typhoon activity, human activities, and sea-level rise. River discharge and sediment load records were compared with the annual expansion of mangrove area into the sea, and a lagged correlation analysis was further conducted using the Pearson coefficient (95 % confidence interval, up to a 15-year lag). Local tidal current characteristics were obtained by integrating published data (Niu, 2019) with remote sensing imagery and visual interpretation. Local wave conditions were analyzed in relation to the estuarine geographic setting. In this

study, a 500 km buffer zone that can completely reflect the influence of typhoons was established (Jiang and Zipser, 2010), and the frequency and maximum wind speeds of typhoons, along with the net mangrove gain, were analyzed to assess their potential relationship. Mangrove degradation induced by human activities was tracked using remote sensing imagery.

2.3.6. Accuracy assessment

The accuracy of the sample points was verified using high-resolution imagery from Google Earth (https://www.google.com/earth/) and Google Street View (https://www.google.com/streetview/). The overall accuracy and Kappa coefficient were used as statistical tools to assess the classification accuracy (Fitzgerald and Lees, 1994). When applying the CCDC classification, sample points were collected every 4 years from 1986 to 2023. The overall accuracy of the mangrove classification exceeded 0.93, and the Kappa coefficient was greater than 0.91 (Table 2), indicating a high level of confidence in the classification results. Additionally, the Digital Shoreline Analysis System was configured with a 95 % confidence interval, further ensuring the robustness of the shoreline change estimates.

3. Results

3.1. Changes in mangrove forest area

The mangrove area presented an overall increase from 38.02 ha in 1986–313.02 ha in 2023, indicating a net growth of 275 ha (Fig. 2A). This growth pattern of the mangrove area was characterized by a slow increase before 1999, followed by a rapid rise until 2023. Specifically, the area expanded at a rate of 3.68 ha/yr from 1986 to 1999, which then accelerated to 12.52 ha/yr between 1999 and 2006 (Fig. 2A). Note that there was a relatively stable phase occurred from 2006 to 2010, during which the mangrove area maintained a mean value of 181.93 ha and the growth rate declined to 4.24 ha/yr (Fig. 2A). Subsequently, the growth rate increased again to 9.42 ha/yr after 2010 (Fig. 2A).

The growth patterns of mangroves of Jiulongjiang Estuary had spatial differences (Fig. 2B-D). In the Northern Section, mangrove area increased slightly from 2.77 ha in 1986–16.88 ha in 2023, while its share of the total mangrove area declined from 7.29 % to 5.39 %. In the Southern Section, mangrove area rose from 15.34 ha to 56.63 ha, but its proportion decreased from 40.35 % to 18.09 %. By contrast, the Central Island Section followed the overall trend, expanding from 19.90 ha to 239.51 ha, with its share increasing from 52.36 % to 76.52 %.

3.2. Spatial gain and loss in mangrove area

Between 1986 and 2023, the mangrove area increased by 319.87 ha, with a total loss of 44.87 ha (Fig. 3A, Fig. 4). The Central Island Section accounted for the majority of mangroves, gaining 245.22 ha and losing 25.61 ha, with 87.78 ha added between 1998 and 2006 in estuarine bays, representing 36 % of its total gain. Losses were concentrated at Haimen Island during 2006–2010 and along the channel in 2018–2023.

Table 2
Accuracy assessment of the research area.

Year	Overall accuracy	Kappa coefficient value
1986	0.98	0.97
1990	0.93	0.91
1994	0.94	0.92
1998	0.96	0.94
2002	0.98	0.97
2006	0.95	0.93
2010	0.96	0.95
2014	0.96	0.95
2018	0.93	0.91
2022	0.99	0.98

The Northern Section remained relatively stable, adding 9.71 ha from 2010 to 2023, mostly along channels and accounting for 55 % of its gain. The Southern Section gained 29.54 ha over the same period, representing 35 % of its increase, with growth primarily along channels, but it experienced early losses of 4.98 ha between 1990 and 1994.

The spatial distribution of mangrove areas in the Northern Section, Central Island Section, and Southern Section exhibited similar patterns over time. For clarity, we define the “bay” as the broader estuarine water body, including the mouths of channels, whereas “channels” refer to the narrower tidal waterways. Mangroves were initially confined to the estuarine bay and subsequently colonized the channels, resulting in a more fragmented distribution over time (Fig. 4). Fig. 3B-D exhibited such transformation. Specifically, between 1986 and 2010, mangrove growth was predominantly concentrated in estuarine bay areas, contributing 94 %, 95 %, and 54 % of the total growth in the Northern Section, Central Island Section, and Southern Section, respectively (Fig. 3B-D). However, from 2010 to 2023, these proportions declined sharply to 11 %, 41 %, and 19 % (Fig. 3B-D), indicating that mangrove forests gradually shifted their main growth areas towards the channels (Fig. 4).

3.3. Shoreline migration of mangrove forests

Analysis of the five mangrove shorelines over the long-term observation period revealed a consistent seaward expansion trend, with no evidence of shoreline loss (Fig. S2). The overall average expansion rate across the 767 transects was found to be 4.36 m/year between 1986 and 2023.

However, the seaward expansion rates of mangrove shorelines vary across different regions. Specifically, the Central Island Section region exhibited the fastest rate of seaward expansion at 5.19 m/year, followed by the Northern Section with a rate of 3.42 m/year. The slowest expansion occurred in the Southern Section, which is significantly below the average rate, with a rate of only 2.57 m/year. In the Central Island Section, mangrove shorelines displayed substantial differences in seaward expansion rates, with Gamvin Farm having the highest rate of 14.92 m/year, while the average rate at Haimen Island and Datu Chau is 1.27 m/year (Fig. S2).

3.4. Changes in landscape patterns of mangrove forests

PD and COHESION exhibited pronounced abrupt changes during the observation period (Fig. 5). In the early stage, PD exhibited a rapid decline, followed by a notable increase after 2011 (Fig. 5A). Similarly, COHESION initially increased rapidly but began to decline after 2011 (Fig. 5B). Specifically, PD declined rapidly from 211.01 in 1986–82.83 in 2011 at a rate of 5.13/yr, followed by an increase to 106.33 in 2023 at a rate of 1.96/yr (Fig. 5A). In contrast, COHESION increased from 78.74 in 1986–92.32 in 2011 at a rate of 0.54/yr, before decreasing to 88.67 in 2023 at a rate of 0.30/yr (Fig. 5B).

3.5. Datasets describing estuary conditions

3.5.1. River discharge and sediment supply

Between 1980 and 1988, sediment discharge of the Jiulongjiang Estuary reached 4.18 million tons, declining to an average of 3.09 million tons after the 1990s, while runoff volume decreased by only 7 % (Fig. 6). Despite this reduction, the annual seaward expansion of mangrove area remained relatively stable across both periods. Notably, peak expansion years in 2002, 2004, and 2011 coincided with particularly low sediment discharge. Lagged correlation analysis revealed no significant relationship between sediment transport and mangrove seaward expansion.

3.5.2. Tidal dynamics and sediment transport

In the outer sea of the estuary, current velocity decreased markedly

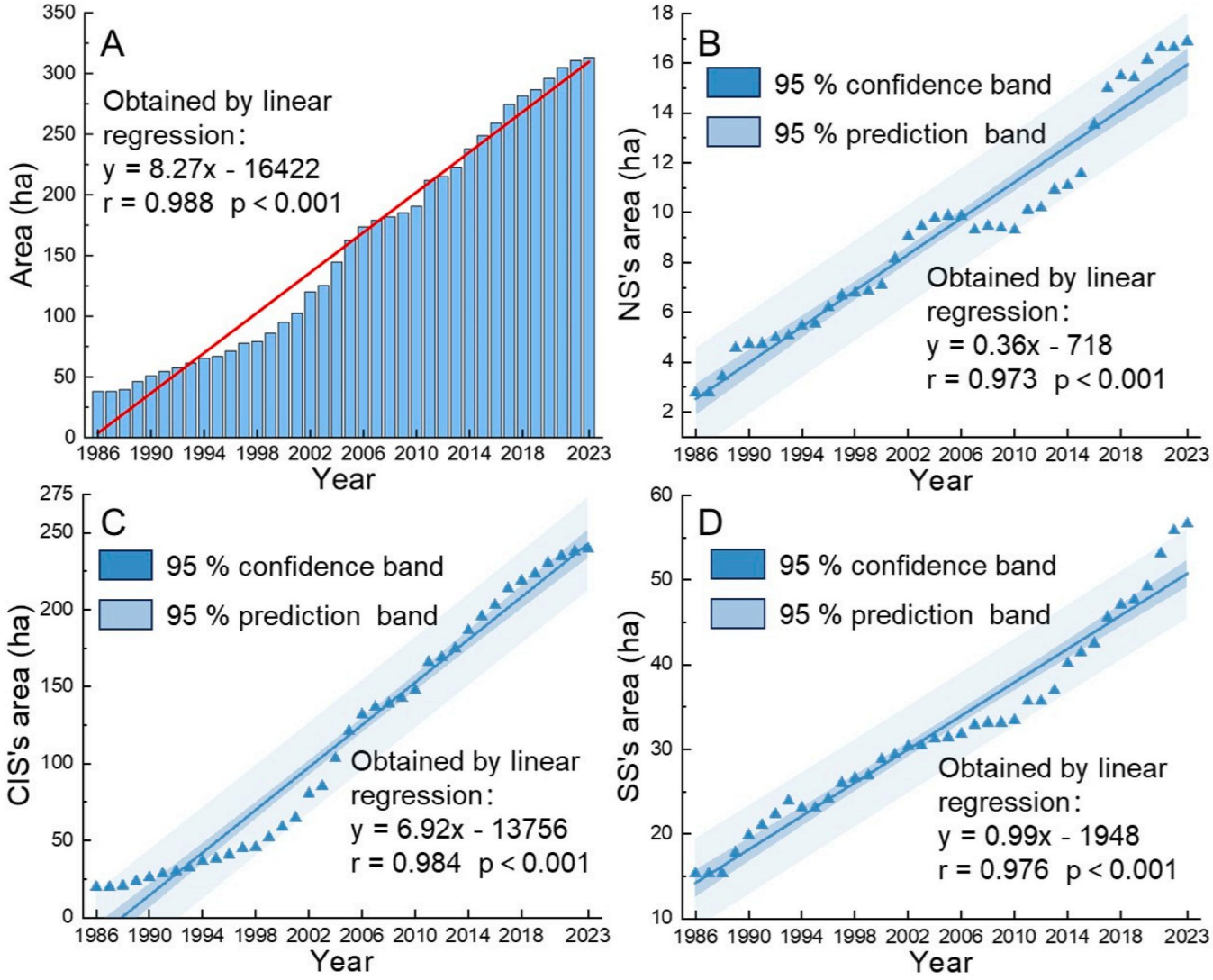

Fig. 2. Temporal and spatial dynamics of mangrove forests in the Jiulongjiang Estuary from 1986 to 2023. (A) Overall temporal changes in total mangrove forest area. (B–D) Mangrove area variations in the Northern Section (B), Central Island Section (C), and Southern Section (D).

from over 1 m/s at the mouth to less than 0.5 m/s within Xiamen Bay (Fig. S3A). Within the estuarine bay, tidal flow primarily followed an east-west direction, largely aligned with the coastline (Fig. S3B). Sediment transport showed seasonal variability: during the flood season, most sediments settled within the bay, whereas in the dry season, suspended sediments were substantially reduced (Fig. S3C).

3.5.3. Wave climate and geomorphic setting

Waves from the east and northeast dominated the outer sea, accounting for 58 % of total wave occurrences, with heights generally exceeding 1 m and peaking at 4.17 m (Fig. S4). Barrier islands around the estuary were generally aligned with the dominant wave directions, while waves from other directions were considerably attenuated before reaching the islands, with heights typically below 1 m (Fig. S4).

3.5.4. Mangrove disturbance factors

From 1999–2023, mangroves generally exhibited rapid growth, with net annual gains of 11.90 ha between 1999 and 2005 and 9.43 ha between 2011 and 2023, while gains between 2006 and 2010 declined to 5.63 ha/yr (Fig. 7). Wind speeds from 2005 to 2008 ranked among the top five highest from 1986 to 2021, with 2006 recording the maximum wind speed and 2008 the highest number of typhoons (Fig. 7). During this period, net annual gains decreased from 17.87 ha in 2005–11.18 ha in 2006, representing the largest single-year decline, and then reached a minimum of 2.77 ha in 2008 (Fig. 7). In addition, human activities, including aquaculture (Fig. S5A), bridge construction (Fig. S5BC), berth development (Fig. S5AD), and wharf construction (Fig. S5E), caused localized mangrove degradation. Along the Fujian coast, sea levels rose at an accelerating rate, representing a long-term pressure on coastal ecosystems (Fig. S6).

4. Discussion

4.1. Drivers of mangrove area dynamics

4.1.1. Mangrove gain

Sediments support mangrove growth by supplying nutrients, improving soil structure, and providing favorable conditions for seedling establishment (Asbridge et al., 2016; Kamal et al., 2020). Adequate sediment enables mangroves to enhance coastal accretion and maintain soil elevation (Turner, 2015), whereas limited upstream supply constrains their erosion-prevention capacity (Besset et al., 2019). Prior to 1990, high sediment discharge from the Jiulongjiang Estuary promoted siltation, raising the delta by 10–15 cm/yr and facilitating seaward expansion of 100–150 m (Cai et al., 1987). After the 1990s, upstream hydraulic structures reduced sediment discharge (Chen et al., 2018;

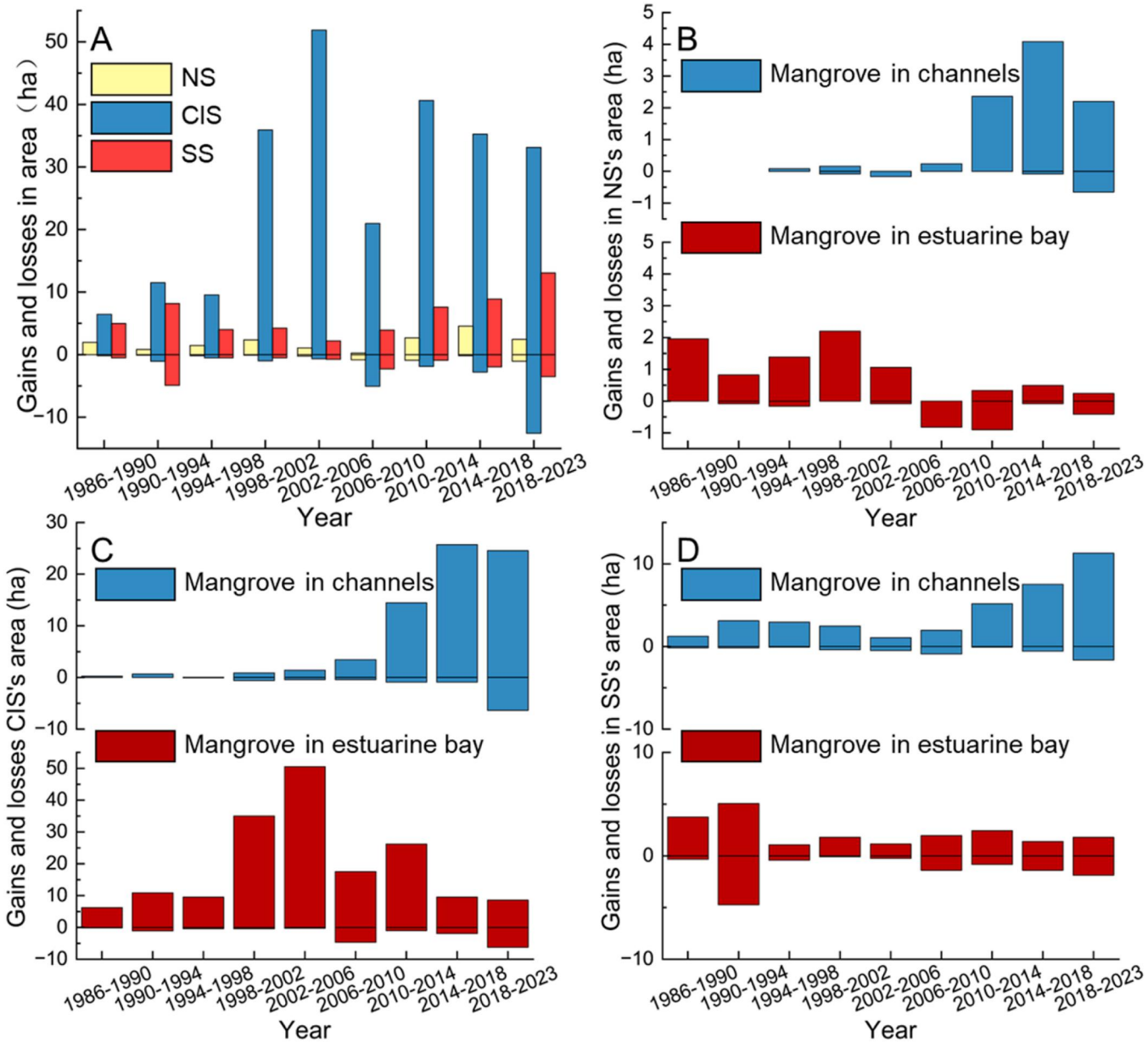

Fig. 3. Spatiotemporal changes in mangrove gains and losses in the Jiulongjiang Estuary from 1986 to 2023. (A) Overall patterns of mangrove area gains and losses. (B–D) Subregional distributions of mangrove changes in estuarine bays and channels of the Northern Section (B), Central Island Section (C), and Southern Section (D).

Fig. 6), yet mangrove area continued to expand. Peak expansion even coincided with particularly low sediment supply, showing no significant lagged response and deviating from the expected positive correlation. This suggests that runoff-driven sediment transport may not be the primary driver of mangrove gain.

In tide-dominated estuaries, tidal currents from the open sea typically drive significant landward sediment transport (Dalrymple and Choi, 2007). The Jiulongjiang Estuary, however, exhibits different dynamics. Complex topography and barrier islands sharply reduce flow velocity (Fig. S3A), limiting the transport of coarse sediments and preventing offshore sediments from entering the bay (Niu, 2019). Consequently, sediment supply in this estuary is primarily derived from terrestrial sources. After 1990, despite a 26.08 % decrease in runoff sediment transport (Fig. 6), mangroves continued to expand in the seaward direction. We speculate that this was largely driven by the resuspension of surface sediments by tidal currents and the landward transport of sediments from Xiamen Bay (Wang, 2005). Within the estuarine bay, flood tides generally flow slightly northward, while ebb tides flow southward, particularly near the entrance where water exchanges with Xiamen Bay (Fig. S3B). This creates a residual surface current that transports sediments west of Haimen Island, depositing them in the central bay, while upstream sediments are directed southeastward, accumulating in the same central region and are partially conveyed into Xiamen Bay (Fig. S3C). These tidal dynamics enable mudflats in mangrove areas to rise steadily, creating conditions suitable for rapid mangrove colonization once an appropriate elevation is reached (Swales et al., 2015). This mechanism explains the observed rapid expansion at Gamvin Farm and Datu Chau, where mangrove areas grew from 13.70 ha in 1986–154.43 ha in 2023, representing 49.34 % of the total mangrove area. Semi-diurnal tides further support this expansion by providing optimal submergence conditions for *Kandelia obovata* (Luzhen et al., 2004). The estuarine coupling process, dominated by tidal currents and supplemented by river discharge, also influences mangrove dynamics. During the flood season, which accounts

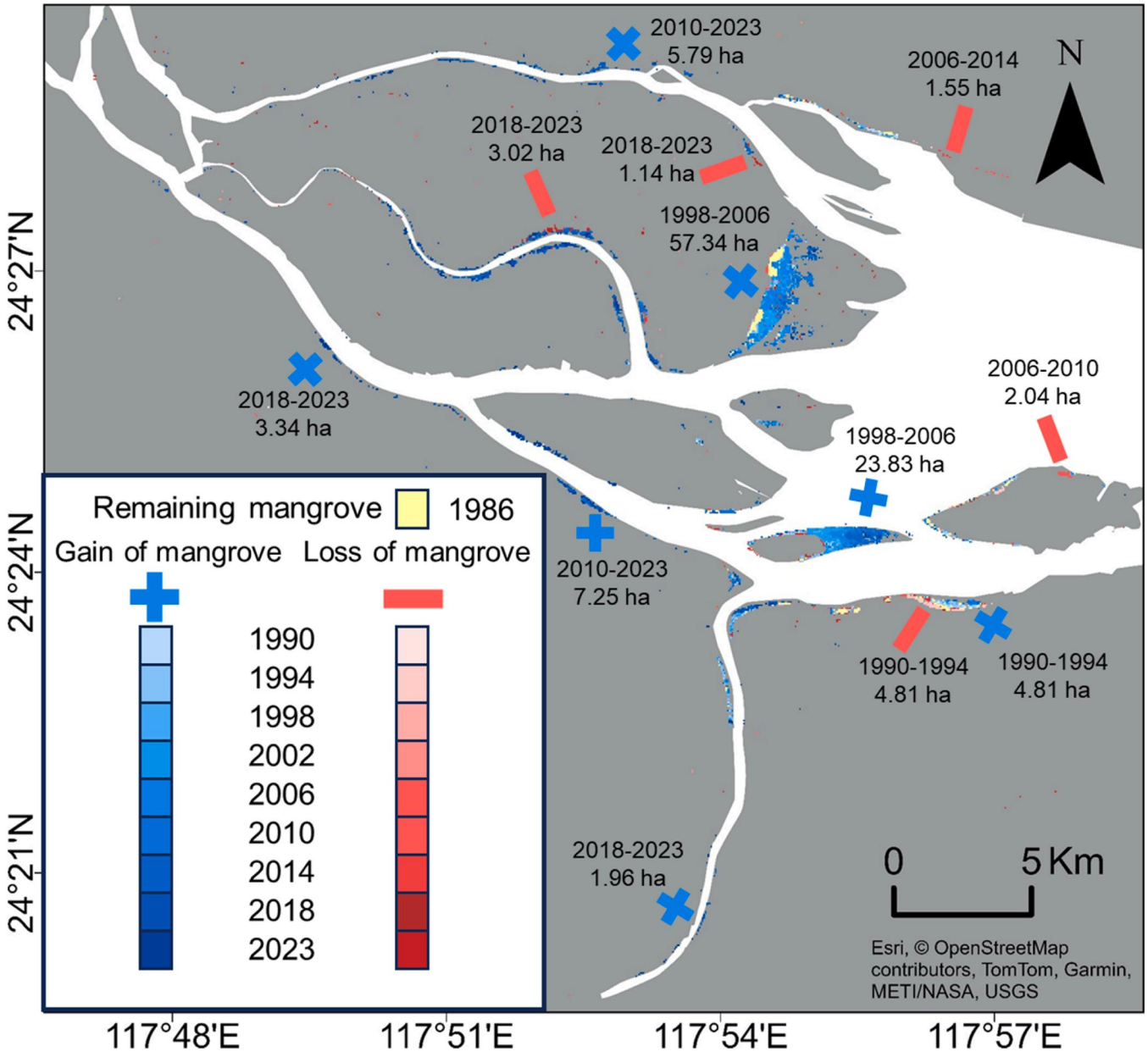

Fig. 4. Spatial distribution of mangrove area loss and gain in Jiulongjian Estuary from 1986 to 2023.

for 75 % of annual runoff (Gao et al., 2018), the tidal limit (the inland boundary where flow slows and sediment accumulates) is located near Gamvin Farm (Yang et al., 2017). In the dry season, reduced runoff enhances tidal intake and sediment transport, shifting the tidal limit upstream into the middle and upper channels (Fig. S3B). This redistribution of sediments creates a favorable environment for mangrove growth, as reduced runoff facilitates tidal sediment redistribution and enhances landward sediment transport (Wells, 1995). Simultaneously, tidal currents deposit sediments within the channels (Fig. S3C), providing a substrate that supports subsequent mangrove expansion. Since 2010, mangroves have emerged at multiple channel locations, increasing by 86.07 ha by 2023 (Fig. 3).

Since 1990, annual investments in mangrove restoration in the Jiulongjiang Estuary have been conducted (Ye et al., 2006), such as the planting of mangroves at Gamvin Farm in 1999 and subsequent projects initiated by the China Mangrove Conservation Network in 2003, which played a pivotal role (Fig. 8 C-E). The sharp decline in PD and the concurrent rise in COHESION indicate an increasing aggregation of mangroves in specific areas (Fig. 5). Additionally, the spur dam in the upper section of the Middle Channel, together with the surrounding topography, diverted a substantial volume of fluvial water into the South Channel, thereby weakening hydrodynamic conditions in the Middle Channel. This alteration contributed to severe siltation in the Middle Channel (Fig. S7), creating favorable conditions for mangrove growth and expansion. Consequently, the Middle Channel exhibited the most extensive mangrove coverage among all channels. During this period, COHESION and PD reached turning points, with COHESION decreasing by 3.64 and PD increasing by 23.97 (Fig. 5).

4.1.2. Mangrove loss

Typhoons significantly affect coastal ecosystems, particularly mangroves, by causing direct physical damage (Kauffman and Cole, 2010). In the Jiulongjiang Estuary, consecutive years of intense typhoons slowed mangrove expansion. Although mangrove areas generally grew rapidly from 1999 to 2023, growth plateaued between 2006 and 2010 (Fig. 7), coinciding with extreme typhoon events from 2005 to 2008. In

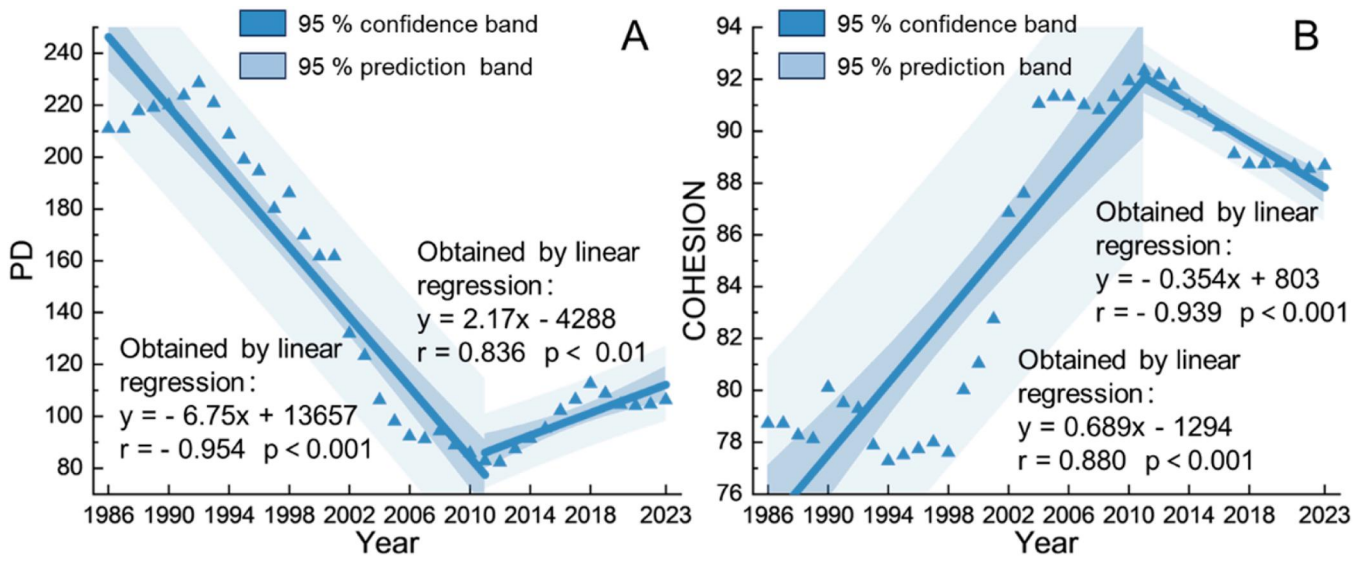

Fig. 5. Changes in landscape indices of mangrove forests in the Jiulongjiang Estuary. (A) Patch Density (PD). (B) COHESION index.

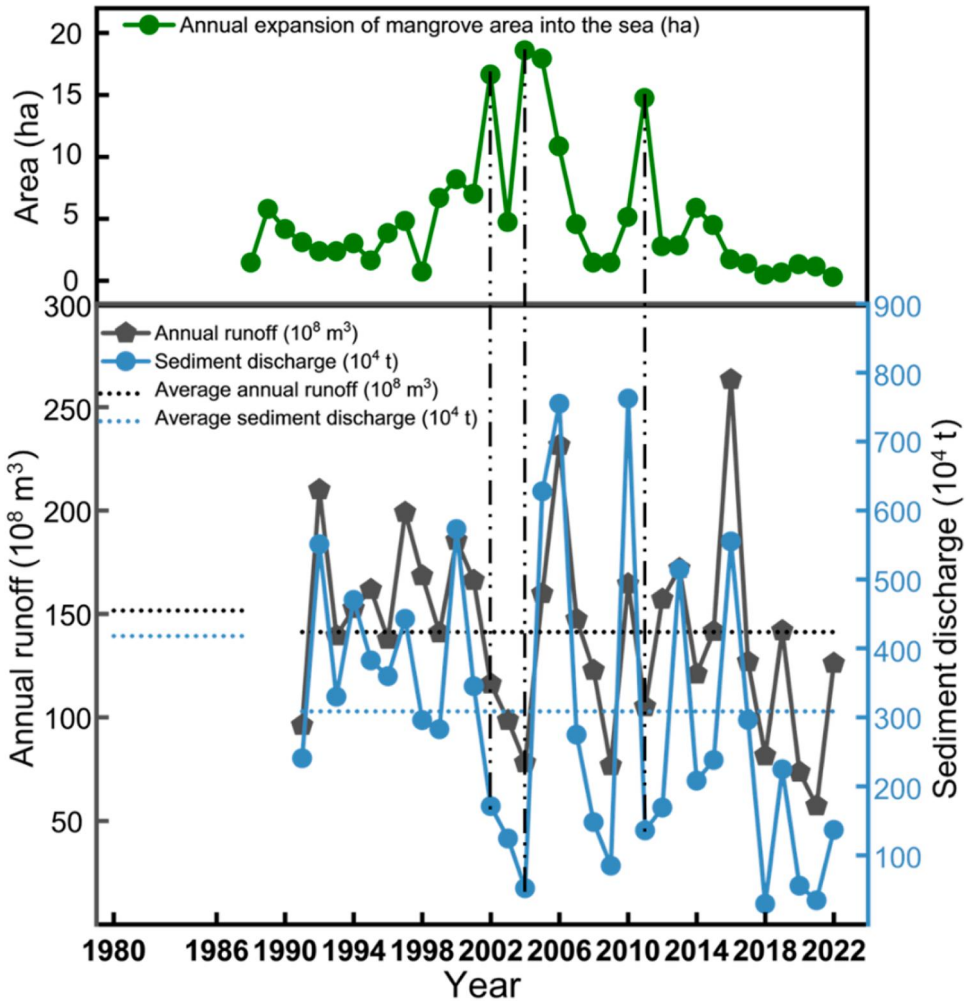

Fig. 6. Annual seaward mangrove expansion in relation to sediment discharge and runoff in the Jiulongjiang Estuary.

2010, ten heavy rainstorms and five typhoons further contributed to substantial damage. Typhoons not only cause direct mechanical injury but also induce secondary damage through drifting debris and broken branches, severely reducing seedling survival at the seaward edge and limiting growth and expansion (Primavera et al., 2016). However, well-established artificial mangrove forests have demonstrated

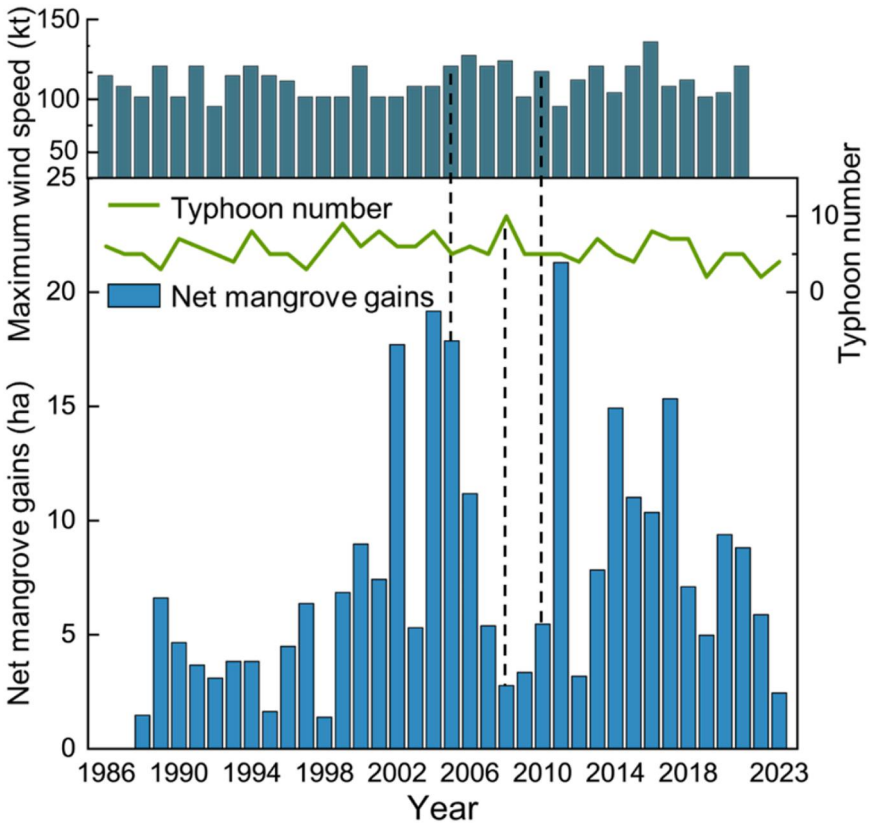

Fig. 7. Net mangrove gains with typhoon number and maximum wind speed.

exceptional resilience even under super typhoons (Zhang et al., 2022). For instance, in 2016, despite a typhoon with maximum wind speeds of 129 kt, net mangrove gains decreased by only 0.65 ha relative to the previous year (Fig. 7), suggesting that, over time, the overall impact of typhoons on mangrove populations in the study area is limited. In addition, the primary driver of mangrove loss in the Jiulongjiang Estuary is the demand to support local urban development and meet the needs of the resident population. Nevertheless, the overall extent of loss remains limited, totaling only 8.24 ha (Fig. S5).

4.2. Drivers of mangrove shoreline dynamics

The mangrove shoreline in the Jiulongjiang Estuary has consistently expanded seaward (Fig. S2). During the flood season, the tidal limit near Gamvin Farm facilitates sediment accumulation along the shoreline, promoting a seaward advance of the mangrove front by 567.02 m (Fig. S3C). While waves can threaten mangrove seedlings and contribute to shoreline degradation (Yuanita.et al., 2021), barrier islands around the estuary, aligned with the dominant wave direction, buffer wave energy effectively (Fig. S4). This protective effect is further enhanced by the estuary's complex bathymetry, where extensive islands and intertidal mudflats in the central region provide natural shelter (Cheng et al., 2020), creating a stable environment conducive to mangrove growth. Within the estuary, waves from the northeast, southeast, and south-southeast, primarily driven by winds (Niu, 2019), influence mangrove distribution. Mangroves in the Southern and Northern Sections, oriented north-south, are largely shielded from direct wave impact, whereas those in the Central Island Section, oriented east-west, benefit from protection by small islands such as Haimen Island. Consequently, shorelines in these areas continue to expand seaward. Additionally, wave action enhances tidal sediment transport from Xiamen Bay, supplementing the estuarine sediment supply. Typhoons during the flood season further increase hydrodynamic forces and sediment deposition; under strong storm conditions, the average suspended sediment concentration rises from 0.1 to 0.25 kg/m^3 (Niu, 2019), facilitating sediment accumulation and supporting continued mangrove expansion.

Moreover, the invasion of *Spartina alterniflora* into mangrove ecosystems, largely resulting from human introduction and deliberate planting, has greatly threatened the ecological integrity of mangrove habitats (Zheng et al., 2023). Since 2014, mangroves at Gamvin Farm have remained relatively stable with minor seaward changes, whereas mangroves in other areas have nearly occupied the entire intertidal zone (Fig. 8). This limited expansion at Gamvin Farm is due to mid-intertidal zones being dominated by *Spartina alterniflora* and other invasive species, which occupy an average area of 19.48 ha, severely hindering mangrove colonization (Fig. 9).

Globally, most mangrove regions are unable to keep pace with rising sea levels, rendering them vulnerable to submersion (Sasmito et al., 2016; Saintilan et al., 2020), with sea level rise projected as a major threat (Lovelock et al., 2015; Blankespoor et al., 2017). In contrast, mangroves in the Jiulongjiang Estuary exhibit a distinct trend of seaward expansion. Along the Fujian coast, sea levels have been rising at an accelerating rate (Fig. S6), with an expected increase of 75–180 mm over the next thirty years (Ministry of Natural Resources. 2024). At the Jiulongjiang Estuary, the rate of sea level rise is 3.1 mm yr^{-1} (Yuan et al., 2016), while the average surface elevation gain of mangroves is 34.1 mm yr^{-1} (Fu, 2019), far exceeding local sea level rise. These observations suggest that, at least in the short term, rising sea levels are unlikely to substantially affect the seaward expansion of the mangrove shoreline.

4.3. Primary drivers and management implications of mangrove dynamics

Ground and historical records (He et al., 2020, September) allow for the delineation of naturally restored mangrove areas, facilitating a more

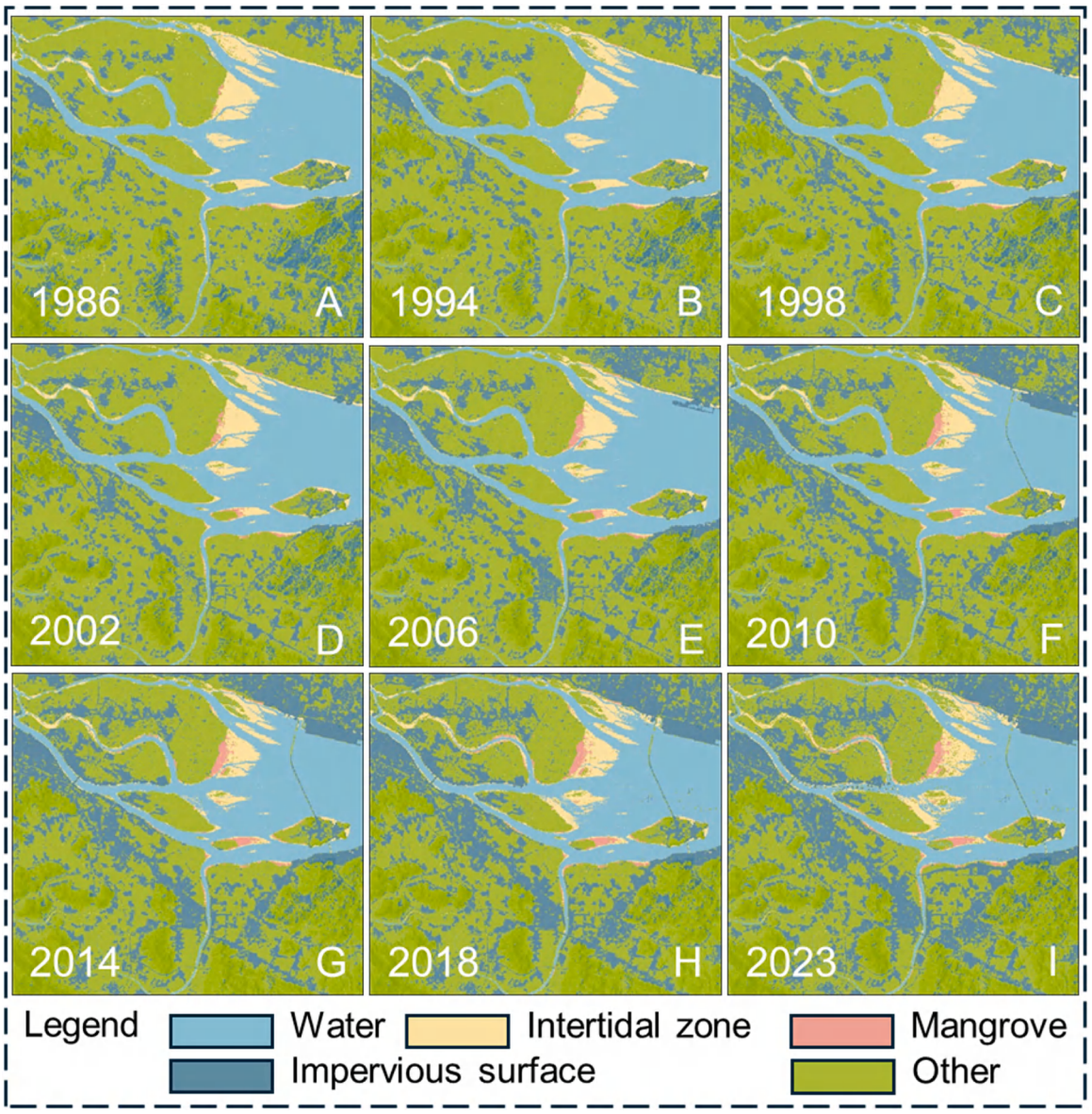

Fig. 8. Temporal and spatial dynamics of mangrove changes in the Jiulongjiang Estuary. A-I: Temporal and spatial dynamics of mangrove changes in different periods from 1986 to 2023.

detailed investigation of the primary drivers of mangrove dynamics. These naturally restored mangrove areas generally exhibit an S-shaped growth curve typical of natural development (Fig. 10); however, they also did not show a significant delayed response to runoff sediment supply, and extreme weather events between 2006 and 2010 caused deviations from the expected trajectory. The average proportion of naturally restored mangroves is 34 %. Although the total mangrove area has continuously increased, this proportion declined from 30 % in 1986–28 % in 2023, showing that human interventions have been the primary driver of mangrove growth in the study area, with planted mangroves concentrated at the tidal limits (Fig. 4), highlighting the ecological importance of these zones. Natural sedimentation at the tidal limits provides stable substrates that support mangrove establishment and expansion. From a management perspective, harnessing this process can reduce reliance on costly interventions and guide restoration efforts. In addition, prioritizing tidal limit areas enables effective monitoring of ecosystem health and enhances coastal resilience to sea-level rise and extreme weather events.

4.4. Uncertainty analysis

This study employed the CCDC method combined with remote sensing imagery to examine the long-term trends and spatiotemporal dynamics of mangroves in the Jiulongjiang Estuary. Although the method is robust, several uncertainties remain, particularly those related to data sources and potential errors during processing. A key limitation is the 30 m spatial resolution of Landsat imagery, which may result in pixel-level errors approaching one square kilometer. Nevertheless, the CCDC approach alleviates this issue by utilizing long-term time series imagery for classification, thereby incorporating the temporal stability of individual pixels rather than relying on single-scene observations that are more prone to random errors. To assess model performance, we applied the Error Matrix Method (Foody, 2002) with independent validation datasets. Overall accuracy and the Kappa coefficient, both ranging from 0 to 1, were used to quantify the agreement between classification results and reference data. Values above 0.8 are generally considered reliable, whereas those below 0.4 indicate poor accuracy (Foody, 2010). In this study, the annual overall accuracy and Kappa coefficient consistently exceeded 0.90 (Table 2), confirming the

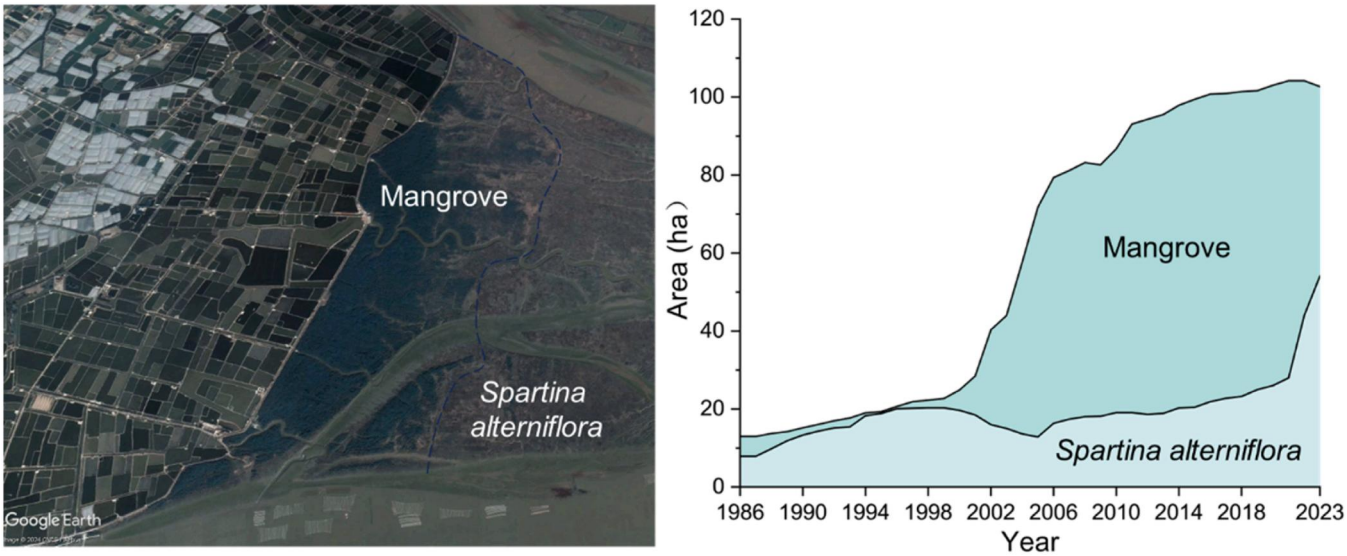

Fig. 9. Vegetation distribution on the intertidal flats of Gamvin Farm. Source: Google Earth (https://www.google.com/earth/).

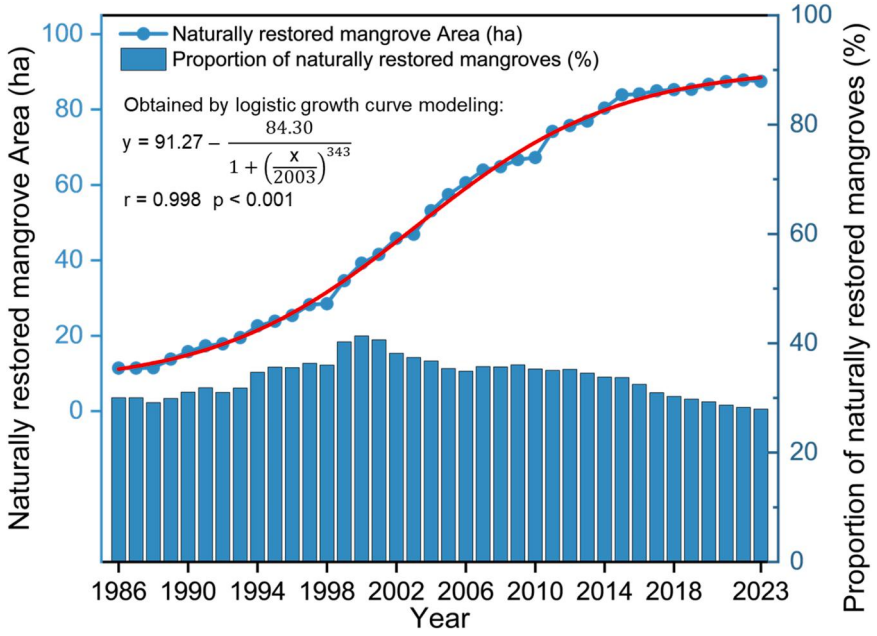

Fig. 10. Naturally restored mangrove area and proportion.

high reliability and robustness of the classification outcomes.

Another source of uncertainty relates to the detectability of planted mangrove seedlings in Landsat imagery. Newly planted seedlings usually require a growth period before reaching a canopy size that can be distinguished at a 30 m spatial resolution, leading to a potential time lag in their appearance in the classification results. However, given that mangrove restoration efforts have been conducted continuously over the years in the study area and that this study focuses on long-term trends rather than short-term fluctuations, the influence of this delayed visibility on the overall results is considered limited.

In this study, wave data from the European Centre for Medium-Range Weather Forecasts (ECMWF) with relatively high spatial and temporal resolution (e.g., hourly) were employed. While the dataset generally provide reliable insights, they may exhibit systematic biases under anomalous climatic events or extreme environmental conditions, potentially influencing conclusions regarding hydrodynamic impacts on mangrove dynamics. Overall, despite the robust analysis presented for the Jiulongjiang Estuary, several uncertainties should be acknowledged, including those related to data resolution, temporal gaps, potential biases in wave and current datasets, and classification procedures. These factors highlight the need for cautious interpretation of the results and underscore the importance of continued methodological refinement.

5. Conclusions

Mangrove forests in Fujian Province, representing one of the northernmost natural mangrove distributions in China, are mainly concentrated in the tide-dominated Jiulongjiang Estuary. This study provides a comprehensive spatiotemporal assessment of mangrove dynamics from 1986 to 2023, revealing both natural and anthropogenic drivers shaping their evolution. The main conclusions are as follows:

1. The mangrove area in the Jiulongjiang Estuary expanded continuously from 1986 to 2023 at an average rate of 7.43 ha/yr, with consistent trends across the three subregions. Early expansion occurred

mainly in estuarine bays, characterized by reduced patch density (PD) and increased COHESION. After 2010, mangroves expanded along estuarine channels, reversing these spatial patterns.

2. Artificial planting and tidal hydrodynamics jointly dominated mangrove expansion. Most planted mangroves were distributed near the tidal limit, where tidal currents enhance sediment redistribution and deposition, providing favorable conditions for colonization. Temporary stagnation from 2006 to 2010 was largely associated with typhoon disturbances, while engineering activities caused localized degradation. Sea-level rise and wave action exerted limited influence on mangrove expansion.

3. Restoration efforts should prioritize the tidal limit zone, where harnessing natural sedimentation processes can promote sustainable mangrove growth, reduce engineering costs, and minimize potential ecological conflicts such as land reclamation.

CRediT authorship contribution statement

Weiming Li: Writing – review & editing, Writing – original draft, Methodology, Investigation, Formal analysis, Data curation. **Zhijun Dai:** Writing – review & editing, Writing – original draft, Visualization, Supervision, Software, Methodology, Formal analysis, Data curation, Conceptualization. **Xu Liu:** Writing – review & editing, Validation, Supervision, Resources, Conceptualization. **Xuefei Mei:** Writing – original draft, Software, Formal analysis, Data curation.

Declaration of Competing Interest

The authors declare that there is no conflicts of interest regarding the submitted paper of “Seaward dynamic changes in mangrove forest over a tide-dominated estuary between 1986 and 2023”.

Acknowledgments

This research was supported by the National Natural Science Key Foundation of China (NSFC) (41930537), Shanghai International Science and Technology Cooperation Fund Project (23230713800 , 24230740100), and the Funds for Ministry of Science and Technology of China (SKLEC).

Appendix A. Supporting information

Supplementary data associated with this article can be found in the online version at doi:10.1016/j.foreco.2025.123370.

Data availability

Data will be made available on request.

References

Allison, M.A., Lee, M.T., 2004. Sediment exchange between Amazon mudbanks and shore-fringing mangroves in French Guiana. Mar. Geol. 208 (2-4), 169–190.
Alongi, D., 2009. The energetics of mangrove forests. Springer Science & Business Media.
Alongi, D.M., 2002. Present state and future of the world’s mangrove forests. Environ. Conserv. 29 (3), 331–349.
Asbridge, E., Lucas, R., Ticehurst, C., Bunting, P., 2016. Mangrove response to environmental change in Australia’s Gulf of Carpentaria. Ecol. Evol. 6 (11), 3523–3539.
Awty-Carroll, K., Bunting, P., Hardy, A., Bell, G., 2021. Evaluation of the Continuous Monitoring of Land Disturbance Algorithm for Large-Scale Mangrove Classification. Remote Sens. 13 (19), 3978.
Balke, T., Swales, A., Lovelock, C.E., Herman, P.M., Bouma, T.J., 2015. Limits to seaward expansion of mangroves: Translating physical disturbance mechanisms into seedling survival gradients. J. Exp. Mar. Biol. Ecol. 467, 16–25.
Baloloy, A.B., Blanco, A.C., Ana, R.R.C.S., Nadaoka, K., 2020. Development and application of a new mangrove vegetation index (MVI) for rapid and accurate mangrove mapping. ISPRS J. Photogramm. Remote Sens. 166, 95–117.
Besset, M., Gratiot, N., Anthony, E.J., Bouchette, F., Goichot, M., Marchesiello, P., 2019. Mangroves and shoreline erosion in the Mekong River delta, Viet Nam. Estuar. Coast. Shelf Sci. 226, 106263.
Blankespoor, B., Dasgupta, S., Lange, G.M., 2017. Mangroves as a protection from storm surges in a changing climate. Ambio 46 (4), 478–491.
Brown, J.F., Tollerud, H.J., Barber, C.P., Zhou, Q., Dwyer, J.L., Vogelmann, J.E., Rover, J., 2020. Lessons learned implementing an operational continuous United States national land change monitoring capability: The Land Change Monitoring, Assessment, and Projection (LCMAP) approach. Remote Sens. Environ. 238, 111356.
Cai, Y.-e, Cheng, W.-j, Cai, A.-z, et al., 1987. Sedimentary environment of Xiamen Bay. Mar. Geol. Quat. Geol. (1), 27–38. (In Chinese with English abstract).
Chandrasekar, K., Sesha Sai, M.V.R., Roy, P.S., Dwevedi, R.S., 2010. Land Surface Water Index (LSWI) response to rainfall and NDVI using the MODIS Vegetation Index product. Int. J. Remote Sens. 31 (15), 3987–4005.
Chen, B., Xiao, X., Li, X., Pan, L., Doughty, R., Ma, J., Giri, C., 2017. A mangrove forest map of China in 2015: Analysis of time series Landsat 7/8 and Sentinel-1A imagery in Google Earth Engine cloud computing platform. ISPRS J. Photogramm. Remote Sens. 131, 104–120.
Chen, Y., Chen, N., Li, Y., Hong, H., 2018. Multi-timescale sediment responses across a human impacted river-estuary system. J. Hydrol. 560, 160–172.
Cheng, P., Yu, F., Chen, N., Wang, A., 2020. Observational study of tidal mixing asymmetry and eddy viscosity-shear covariance-induced residual flow in the Jiulong River estuary. Cont. Shelf Res. 193, 104035.
Cummings, A.R., Shah, M., 2017. Mangroves in the global climate and environmental mix. Geogr. Compass 12, e12353.
Dai, Z., Long, C., Mei, X., Fagherazzi, S., Xiong, Y., 2024. Overestimation of mangroves deterioration from sea level rise in tropical deltas. Geophys. Res. Lett. 51 (19) e2024GL109675.
Dalrymple, R.W., Choi, K., 2007. Morphologic and facies trends through the fluvial–marine transition in tide-dominated depositional systems: a schematic framework for environmental and sequence-stratigraphic interpretation. EarthSci. Rev. 81 (3-4), 135–174.
Dwyer, J.L., Roy, D.P., Sauer, B., Jenkerson, C.B., Zhang, H.K., Lymburner, L., 2018. Analysis ready data: enabling analysis of the Landsat archive. Remote Sens. 10 (9), 1363.
Feller, I.C., Lovelock, C.E., Berger, U., McKee, K.L., Joye, S.B., Ball, M.C., 2010. Biocomplexity in mangrove ecosystems. Annu. Rev. Mar. Sci. 2 (1), 395–417.
Ferreira, A.C., Borges, R., de Lacerda, L.D., 2022. Can sustainable development save mangroves? Sustainability 14 (3), 1263.
Fitzgerald, R.W., Lees, B.G., 1994. Assessing the classification accuracy of multisource remote sensing data. Remote Sens. Environ. 47 (3), 362–368.
Foody, G.M., 2002. Status of land cover classification accuracy assessment. Remote Sens. Environ. 80 (1), 185–201.
Foody, G.M., 2010. Assessing the accuracy of land cover change with imperfect ground reference data. Remote Sens. Environ. 114 (10), 2271–2285.
Fu, H., 2019. The surface elevation changes of mangrove forests in. China Impacts seaLev. rise Mangrove For. (Dr. Diss.). Xiamen Univ. (In Chinese with English abstract).
Gao, X., Chen, N., Yu, D., Wu, Y., Huang, B., 2018. Hydrological controls on nitrogen (ammonium versus nitrate) fluxes from river to coast in a subtropical region: Observation and modeling. J. Environ. Manag. 213, 382–391.
Godoy, M.D., Lacerda, L.D.D., 2015. Mangroves response to climate change: a review of recent findings on mangrove extension and distribution. An. da Acad. Bras. De. Ciências 87 (2), 651–667.
Goldberg, L., Lagomasino, D., Thomas, N., Fatoyinbo, T., 2020. Global declines in human-driven mangrove loss. Glob. Change Biol. 26 (10), 5844–5855.
He, Y., Zhang, T., You, S., Luo, Z., Zhang, X., & Zhang, R. (2020, September). Remote sensing monitoring of mangrove variation in jiulong river estuary of fujian from 1978 to 2018. In IGARSS 2020-2020 IEEE International Geoscience and Remote Sensing Symposium (pp. 6654-6657). IEEE.
Hersbach, H., Bell, B., Berrisford, P., Horányi, A., Muñoz-Sabater, J., Nicolas, J., Peubey, C., Radu, R., Schepers, D., Simmons, A., Soci, C., & Thépaut, J.N. (2018). ERA5 hourly data on single levels from 1979 to present. Copernicus Climate Change Service (C3S) Climate Data Store (CDS).
Jiang, H., Zipser, E.J., 2010. Contribution of tropical cyclones to the global precipitation from eight seasons of TRMM data: Regional, seasonal, and interannual variations. J. Clim. 23 (6), 1526–1543.
Jiang, Y.W., Wai, O.W., 2005. Drying–wetting approach for 3D finite element sigma coordinate model for estuaries with large tidal flats. Adv. Water Resour. 28 (8), 779–792.
Kamal, A.H.M., Hoque, M.M., Idris, M.H., Billah, M.M., Karim, N.U., Bhuiyan, M.K.A., 2020. Nutrient properties of tidal-borne alluvial sediments from a tropical mangrove ecosystem. Reg. Stud. Mar. Sci. 36, 101299.
Kamil, E.A., Takaijudin, H., Hashim, A.M., 2021. Mangroves as coastal bio-shield: a review of mangroves performance in wave attenuation. Civ. Eng. J. 7 (11), 1964–1981.
Kauffman, J.B., Cole, T.G., 2010. Micronesian mangrove forest structure and tree responses to a severe typhoon. Wetlands 30, 1077–1084.
Krauss, K.W., Osland, M.J., 2020. Tropical cyclones and the organization of mangrove forests: a review. Ann. Bot. 125 (2), 213–234.
Kuenzer, C., Bluemel, A., Gebhardt, S., Quoc, T.V., Dech, S., 2011. Remote sensing of mangrove ecosystems: A review. Remote Sens. 3 (5), 878–928.
Lee, S.Y., Primavera, J.H., Dahdouh-Guebas, F., McKee, K., Bosire, J.O., Cannicci, S., Record, S., 2014. Ecological role and services of tropical mangrove ecosystems: a reassessment. Glob. Ecol. Biogeogr. 23 (7), 726–743.

Lewis III, R.R., Milbrandt, E.C., Brown, B., Krauss, K.W., Rovai, A.S., Beever III, J.W., Flynn, L.L., 2016. Stress in mangrove forests: Early detection and preemptive rehabilitation are essential for future successful worldwide mangrove forest management. Mar. Pollut. Bull. 109 (2), 764–771.
Long, C., Dai, Z., Zhou, X., Mei, X., Van, C.M., 2021. Mapping mangrove forests in the red river delta, vietnam. For. Ecol. Manag. 483, 118910.
López, L., Cellone, F., 2022. SfM-MVS and GIS analysis of shoreline changes in a coastal wetland, Parque Costero del Sur biosphere reserve, Argentina. Geocarto Int. 37 (26), 11134–11150.
Lovelock, C.E., 2020. Blue carbon from the past forecasts the future. Science 368 (6495), 1050–1052.
Lovelock, C.E., Bennion, V., Grinham, A., Cahoon, D.R., 2011. The role of surface and subsurface processes in keeping pace with sea level rise in intertidal wetlands of Moreton Bay, Queensland, Australia. Ecosystems 14, 745–757.
Lovelock, C.E., Cahoon, D.R., Friess, D.A., Guntenspergen, G.R., Krauss, K.W., Reef, R., Triet, T., 2015. The vulnerability of Indo-Pacific mangrove forests to sea-level rise. Nature 526 (7574), 559–563.
Luzhen, C., Wenqing, W., Peng, L.I.N., 2004. Influence of water logging time on the growth of *Kandelia candel* seedlings. Acta Oceanol. Sin. (1), 149–158.
Malini, B.H., Rao, K.N., 2004. Coastal erosion and habitat loss along the Godavari delta front- a fallout of dam construction (?). Curr. Sci. 87 (9), 1232–1236.
McGarigal, K., 2006. Landscape pattern metrics. Encycl. environmetrics.
McGarigal, K., Marks, B.J., 1995. Spatial pattern analysis program for quantifying landscape structure. In: Gen. Tech. Rep. PNW-GTR-351., 10. US Department of Agriculture, Forest Service, Pacific Northwest Research Station, pp. 1–122.
Ministry of Natural Resources, 2024. 2023 China Sea Level Bulletin. National Marine Data and Information Service, Tianjin, China. (In Chinese).
Mo, Q., Chen, N., Zhou, X., Chen, J., Duan, S., 2016. Ammonium and phosphate enrichment across the dry–wet transition and their ecological relevance in a subtropical reservoir, China. Environmental Science Processes Impacts 18 (7), 882–894.
Nepita-Villanueva, M.R., Berlanga-Robles, C.A., Ruiz-Luna, A., Morales Barcenas, J.H., 2019. Spatio-temporal mangrove canopy variation (2001–2016) assessed using the MODIS enhanced vegetation index (EVI). J. Coast. Conserv. 23, 589–597.
Niu, J.-S., 2019. The study of suspended sediment distribution and deposition under wave-current interactions of Xiamen Bay (Doctoral dissertation). Xiamen University. (In Chinese with English abstract).
Pengra, B., Gallant, A.L., Zhu, Z., Dahal, D., 2016. Evaluation of the initial thematic output from a continuous change-detection algorithm for use in automated operational land-change mapping by the US Geological Survey. Remote Sens. 8 (10), 811.
Pham, L.T., Vo, T.Q., Dang, T.D., Nguyen, U.T., 2019. Monitoring mangrove association changes in the Can Gio biosphere reserve and implications for management. Remote Sens. Appl. Soc. Environ. 13, 298–305.
Polidoro, B.A., Carpenter, K.E., Collins, L., Duke, N.C., Ellison, A.M., Ellison, J.C., Yong, J.W.H., 2010. The loss of species: mangrove extinction risk and geographic areas of global concern. PloS One 5 (4), e10095.
Primavera, J.H., Dela Cruz, M., Montilijao, C., Consunji, H., Dela Paz, M., Rollon, R.N., Blanco, A., 2016. Preliminary assessment of post-Haiyan mangrove damage and short-term recovery in Eastern Samar, central Philippines. Mar. Pollut. Bull. 109 (2), 744–750.
Rahman, A.F., Dragoni, D., Didan, K., Barreto-Munoz, A., Hutabarat, J.A., 2013. Detecting large scale conversion of mangroves to aquaculture with change point and mixed-pixel analyses of high-fidelity MODIS data. Remote Sens. Environ. 130, 96–107.
Saintilan, N., Khan, N.S., Ashe, E., Kelleway, J.J., Rogers, K., Woodroffe, C.D., Horton, B. P., 2020. Thresholds of mangrove survival under rapid sea level rise. Science 368 (6495), 1118–1121.
Sánchez-Núñez, D.A., Bernal, G., Mancera Pineda, J.E., 2019. The relative role of mangroves on wave erosion mitigation and sediment properties. Estuaries Coasts 42, 2124–2138.
Sasmito, S.D., Murdiyarso, D., Friess, D.A., Kurnianto, S., 2016. Can mangroves keep pace with contemporary sea level rise? A global data review. Wetl. Ecol. Manag. 24, 263–278.
Siachalou, S., Mallinis, G., Tsakiri-Strati, M., 2017. Analysis of time-series spectral index data to enhance crop identification over a Mediterranean rural landscape. IEEE Geosci. Remote Sens. Lett. 14 (9), 1508–1512.
Sippo, J.Z., Lovelock, C.E., Santos, I.R., Sanders, C.J., Maher, D.T., 2018. Mangrove mortality in a changing climate: An overview. Estuar. Coast. Shelf Sci. 215, 241–249.
Suratman, M.N., 2008. Carbon sequestration potential of mangroves in Southeast Asia. In Managing forest ecosystems: The challenge of climate change. Springer Netherlands, Dordrecht, pp. 297–315.
Swales, A., Bentley Sr, S.J., Lovelock, C.E., 2015. Mangrove-forest evolution in a sediment-rich estuarine system: opportunists or agents of geomorphic change? Earth Surf. Process. Landf. 40 (12), 1672–1687.
Temmerman, S., Horstman, E.M., Krauss, K.W., Mullarney, J.C., Pelckmans, I., Schoutens, K., 2023. Marshes and mangroves as nature-based coastal storm buffers. Annu. Rev. Mar. Sci. 15 (1), 95–118.
Tian, Y., Huang, H., Zhou, G., Zhang, Q., Xie, X., Ou, J., Lin, J., 2023. Mangrove biodiversity assessment using UAV LiDAR and hyperspectral data in China's Pinglu canal estuary. Remote Sens. 15 (10), 2622.
Turner, M., 2015. Mangrove maintenance. Nature 526 (7574), 515. -515.
Walsh, J.P., Nittrouer, C.A., 2004. Mangrove-bank sedimentation in a mesotidal environment with large sediment supply, Gulf of Papua. Mar. Geol. 208 (2-4), 225–248.
Wang, J.-Y., Jiang, Y.-W., 2013. The distribution of salinity and the dynamic process of salt flux in Jiulong River Estuary. J. Xiamen Univ. (Nat. Sci.) 52 (6), 7 (In Chinese with English abstract).
Wang, K., Yang, Y., Reniers, G., Huang, Q., 2021. A study into the spatiotemporal distribution of typhoon storm surge disasters in China. Nat. Hazards 108, 1237–1256.
Wang, W., Zhao, M., Deng, C., Lin, P., 2000. Species and its distribution of mangroves in Fujian coastal area. J. Oceanogr. Taiwan Strait 20 (4), 534–540 (In Chinese with English abstract).
Wang, Y., 2005. Initiative research on the transportation of suspended sediments in Jiulongjiang River estuary, Fujian Province, at both flood and low water seasons (Doctoral dissertation). Ocean University of China. (In Chinese with English abstract).
Wang, Y.P., Voulgaris, G., Li, Y., Yang, Y., Gao, J., Chen, J., Gao, S., 2013. Sediment resuspension, flocculation, and settling in a macrotidal estuary. J. Geophys. Res. Oceans 118 (10), 5591–5608.
Wang, Y.S., Gu, J.D., 2021. Ecological responses, adaptation and mechanisms of mangrove wetland ecosystem to global climate change and anthropogenic activities. Int. Biodeterior. Biodegrad. 162, 105248.
Wells, J.T., 1995. Tide-dominated estuaries and tidal rivers. In: In Developments in sedimentology, 53. Elsevier, pp. 179–205.
Worthington, T.A., Andradi-Brown, D.A., Bhargava, R., Buelow, C., Bunting, P., Duncan, C., … & Spalding, M. (2020). Harnessing big data to support the conservation and rehabilitation of mangrove forests globally. One Earth 2 (5): 429-443.
Wu, M.J., Xu, B., Guo, Y.W., 2022. Unusual secondary metabolites from the mangrove ecosystems: Structures, bioactivities, chemical, and bio-syntheses. Mar. Drugs 20 (8), 535.
Wu, R., Dai, Z., Mei, X., Luo, J., Fagherazzi, S., 2025. Profiling of mangrove forest dynamics in the Fly River delta, Papua New Guinea. Mar. Pollut. Bull. 217, 118119.
Xu, Y., Cai, F., Lu, H., Wu, C., Zheng, Y., Bao, J., 2014. The characteristics of linear sands off Minjiang Estuary and Jiulongjiang Estuary in Fujian, China. Acta Oceanol. Sinica. (In Chinese with English abstract).
Yang, S.-l., Lin, L., Hu, C.-y., 2017. Change of flow characteristics at Jiulongjiang estuary under different runoff. Water Resour. Power 35 (7), 52–57 (In Chinese with English abstract).
Ye, J., Lin, G., Zhang, M., Gao, L., 2020. Hazard analysis of typhoon disaster-causing factors based on different landing paths: A case study of Fujian Province, China. Nat. Hazards 100, 811–828.
Ye, Y., Weng, J., Lu, C.-Y., et al., 2006. Mangrove biodiversity restoration. Acta Ecol. Sinica. 26 (4), 1243–1250 (In Chinese with English abstract).
Yuan, F.-C., Zhang, W.-Z., Yang, J.-X., Chen, D.-W., 2016. Study on sea level variability in offshore Fujian. J. Appl. Oceanogr. 35 (1), 20–32 (In Chinese with English abstract).
Yuanita, N., Kurniawan, A., Nurmansyah, I.M., Rizaldi, F.M., 2021. A physical model simulation of combination of a geo-bag dike and mangrove vegetation as a natural coastal protection system for the Indonesian shoreline. Appl. Ocean Res. 108, 102516.
Zeng, Z., Wu, Y., Chen, Z., Huang, Q., Wang, Y., Luo, Y., 2022. Runoff Estimation of Jiulong River Based on Acoustic Doppler Current Profiler Online Monitoring Data and Its Implication for Pollutant Flux Estimation. Int. J. Environ. Res. Public Health 19 (23), 16363.
Zhang, R., Lin, P., 1984. Studies on the flora of mangrove-plants from the coast of China. J. Xiamen Univ. (Nat. Sci.) 33 (2), 232–239+266.
Zhang, X., Treitz, P.M., Chen, D., Quan, C., Shi, L., Li, X., 2017. Mapping mangrove forests using multi-tidal remotely-sensed data and a decision-tree-based procedure. Int. J. Appl. earth Obs. Geoinf. 62, 201–214.
Zhang, X., Lin, P., Chen, X., 2022. Coastal protection by planted mangrove forest during typhoon mangkhut. J. Mar. Sci. Eng. 10 (9), 1288.
Zhang, J., Yang, X., Wang, Z., Zhang, T., Liu, X., 2021. Remote sensing based spatial-temporal monitoring of the changes in coastline mangrove forests in China over the last 40 years. Remote Sens. 13 (10), 1986.
Zheng, J., Wei, H., Chen, R., Liu, J., Wang, L., Gu, W., 2023. Invasive trends of *Spartina alterniflora* in the southeastern Coast of China and potential distributional impacts on mangrove forests. Plants 12 (10), 1923.
Zhou, Y., Dai, Z., Liang, X., Cheng, J., 2024. Machine learning-based monitoring of mangrove ecosystem dynamics in the Indus Delta. For. Ecol. Manag. 571, 122231.
Zhu, Z., Woodcock, C.E., 2014. Continuous change detection and classification of land cover using all available Landsat data. Remote Sens. Environ. 144, 152–171.
Zhu, Z., Gallant, A.L., Woodcock, C.E., Pengra, B., Olofsson, P., Loveland, T.R., Auch, R. F., 2016. Optimizing selection of training and auxiliary data for operational land cover classification for the LCMAP initiative. ISPRS J. Photogramm. Remote Sens. 122, 206–221.